Control of emergent magnetic monopole currents in artificial spin ice

H. Arava [1,2,*] E. Y. Vedmedenko,[3,†] J. Cui [1,2] J. Vijayakumar [4] A. Kleibert [4] and L. J. Heyderman [1,2,‡]

[1]*Laboratory for Mesoscopic Systems, Department of Materials, ETH Zurich, 8093 Zurich, Switzerland*
[2]*Laboratory for Multiscale Materials Experiments, Paul Scherrer Institute, 5232 Villigen PSI, Switzerland*
[3]*Department of Physics, University of Hamburg, 20355 Hamburg, Germany*
[4]*Swiss Light Source, Paul Scherrer Institute, 5232 Villigen PSI, Switzerland*

The control of emergent magnetic monopoles for the generation of monopole currents in artificial spin ice is essential for their use in nanomagnet-based device applications. Here we present a scheme to inject monopole currents into an artificial square ice at specific locations, which provides a means to control the propagation of the generated emergent monopole currents. Specifically, we modify an artificial square ice by populating two of its edges with different vertex configurations consisting of two, three, and four nanomagnets meeting at a common point. After setting an initial state with a global magnetic field, injection of monopoles occurs at one of the edges where the vertices have higher switching probability. We experimentally observe this vertex-specific nucleation of emergent magnetic monopoles using x-ray photoemission electron microscopy. Additionally, we demonstrate that a lateral shift in the reversal of the magnets, leading to the formation of large domains, is consistent with theoretical simulations incorporating higher-order contributions in the magnetic Hamiltonian. Finally, we find a strong correlation between the location of emergent monopole injection and the film thickness, which is a result of the switching probability associated with the different vertex configurations.

I. INTRODUCTION

Artificial spin ice [1–3] consists of arrays of single-domain nanomagnets arranged on different lattices, such as the square [4–6] or kagome [7,8] lattice. In particular, the artificial square ice is a tessellation of a unit cell containing four nanomagnets placed at a common vertex or a four-magnet vertex (see Fig. 1). Mapping the moments associated with each magnet onto a stretched magnetic charge dumbbell [9,10] with opposite charges residing on neighboring vertices, we obtain magnetic moment configurations where the total charge at a four-magnet vertex can be zero (configurations $v4\text{-}1$ and $v4\text{-}2$ in Fig. 1) or nonzero (intermediate $v4\text{-}X$ state in Fig. 1). Such moment configurations (or vertex configurations) with an excess magnetic charge can be considered to be emergent magnetic monopoles, although it should be pointed out that, on a 2D lattice, the artificial square ice does not possess a true Coulomb phase [11,12] and the monopolelike charges are confined by a string tension, and are therefore often referred to as bound monopoles [6,13].

In order to comprehend the behavior of these bound monopoles, their creation and annihilation was first described using a potential-energy function, which has a strong correlation with the lattice spacing of a nanomagnet array [6]. Subsequently, the creation and separation of monopoles in artificial kagome spin ice in an applied magnetic field was experimentally demonstrated [10,14], as well as in a thermally active artificial square ice after removal of an applied magnetic field that was used to obtain an initial remanent state [5]. The dynamics involving the separation of a monopole-antimonopole pair can be characterized as magnetic current or magnetricity [15]. Such magnetic currents are of interest for next-generation devices such as magnetic logic [16,17] and neuromorphic computing [18]. In particular, computation with nanomagnets may provide a low-power alternative to traditional complementary metal oxide semiconductor (CMOS) technology [19,20]. Moreover, an artificial spin-ice structure is inherently complex in nature and may provide an ideal playground to mimic the human brain. However, to exploit the moving charges in devices, it is important to be able to control their injection, in particular the location of their nucleation and the subsequent propagation direction. To this aim, it has been demonstrated that, with careful modification of the shape of specific nanomagnets, which alters the magnetic shape anisotropy and therefore the switching field, sources (lower shape anisotropy) and sinks (higher shape anisotropy) of monopole currents can be created [21]. Likewise, changing the thickness of the nanomagnets alters the energy barrier associated with the switching probability, and therefore is an additional parameter that can be used to tune the probability of nucleation. It should also be noted that the high-frequency response of artificial spin ices is an active field of interest, in which the generation and controlled displacement of monopole-antimonopole pairs could have potential applications as reconfigurable magnonic crystals [22–24].

Furthermore, it has been shown that, in theory, controlled injection of monopoles at a specific location can be achieved

———————
*hanu.arava@gmail.com
†vedmeden@physnet.uni-hamburg.de
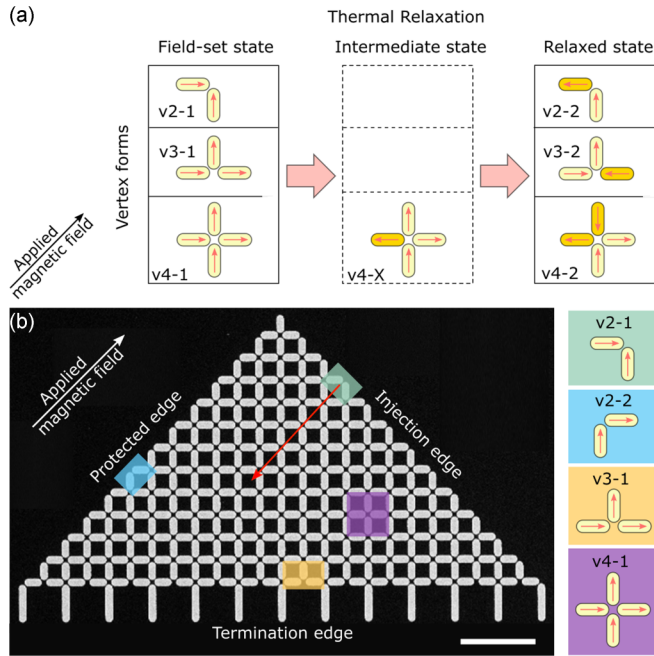‡laura.heyderman@psi.ch

FIG. 1. Vertex forms in an artificial square ice with defined vertex edges. (a) Possible vertex forms at the edges in their initial field-set state and final relaxed state, including the intermediate state for $v4$. (b) A scanning electron microscope image of the $v2$-$v4$ artificial square-ice structure. Shown in the inset are different vertex forms, assuming that the magnetic state has been set with a globally applied magnetic field. It is expected that the $v2$-2 configurations (protected edge) will remain stable throughout a relaxation experiment, while injection of monopoles is highly probable at the $v2$-1 configurations (injection edge) and the generated monopole currents would terminate at the $v3$-1/$v4$-1 configurations (termination edge). The termination edge is denoted by $v4$-1* for brevity with the asterisk indicating the longer-edge nanomagnets. The direction of monopole current propagation is indicated by the red arrow. Scale bar is $2\,\mu$m.

in an artificial square ice when the dipolar coupling strength between two nanomagnets is lowered [25] and when a particular edge is populated with nanomagnets possessing a different magnetic dipole moment compared to the rest of the array [13]. It has also been proposed that the use of heat generated by metal strip lines adjacent to two sides of a square lattice can be used to create unidirectional currents [26]. Other possible avenues to produce controlled injection of monopole currents include the incorporation of topological defects in an artificial square ice [27] and the use of domain walls in connected artificial kagome ice [28]. However, despite the many experimental attempts, there has not been a well-defined scheme to control the location, generation, and directionality of monopole currents [29–31]. Here, we demonstrate the controlled nucleation of monopoles from one edge of an artificial square ice, leading to directional monopole currents, and explain the formation of the generated monopole currents.

II. DESIGN OF THE STRUCTURE

To generate controlled monopole currents, we design an artificial square ice with edges along different directions resulting in different vertex forms corresponding to the number

of nanomagnets meeting at a common point. The possible vertex forms for a square ice are shown in Fig. 1(a). Here we introduce the terminology of a vn-ξ configuration or site where n is the number of nanomagnets at a vertex ($n = 2, 3,$ or 4) and ξ refers to the moment configuration ($\xi = 1$ or 2), with 1 corresponding to a field-set state and 2 to a relaxed low-energy state. With analytical calculations of the dipolar coupling strength using a simple magnetic Hamiltonian [32,33], it can be shown that the difference in energy from an initial field-set state to a state that is a single nanomagnet reversal away (ΔE) is different for each vertex form at the sample edge [Fig. 1(a)]. With this in mind, an artificial square ice is designed where the injection probability at one of the edges is much higher (ΔE is much lower). Specifically, one of its edges contains a $v2$-1 configuration (lower ΔE) and the other has a mixed $v3$-1/$v4$-1 configuration with higher ΔE [Fig. 1(b)]. We refer to this modified square-ice structure as a $v2$-$v4$ structure. For such an asymmetric design, there is a high probability of injection of monopoles at the $v2$-1 configuration edge, which would result in a monopole current that terminates at the $v3$-1/$v4$-1 configuration edge. For brevity, we refer to this termination edge as a $v4$-1* configuration. Here, we use longer nanomagnets as part of the $v4$-1* sites which have a large energy barrier and therefore they remain pinned in their initial moment orientation during a relaxation protocol. As a result, the design of the $v2$-$v4$ structure had to be modified to incorporate a $v4$-1* edge to facilitate ground-state ordering upon thermal relaxation. In addition, the use of longer nanomagnets ensures that injection events are solely restricted to the $v2$-1 sites.

III. METHODS

Artificial square-ice structures consisting of arrays of Permalloy ($Ni_{80}Fe_{20}$) nanomagnets arranged on a square lattice were fabricated on a silicon substrate using electron-beam lithography. The Permalloy thin film was deposited using thermal evaporation at a chamber base pressure of 2×10^{-6} mbar and, in order to obtain structures with different thicknesses, a wedge film was deposited with a thickness ranging from 1 to 15 nm across a distance of 6 mm. The nanomagnets were capped with a thin ($\sim$2 nm) aluminum film to mitigate oxidation of Permalloy. The nanomagnets had dimensions of length $L = 470$ nm and width $W = 200$ nm, and the lattice spacing was 600 nm (center to center distance between two opposing nanomagnets). The lateral dimensions of the longer nanomagnets were $L = 1000$ nm and $W = 200$ nm.

The experiments were performed using x-ray photoemission electron microscopy (X-PEEM) at the Surface/Interface microscopy beamline, Swiss Light Source. Magnetic contrast images were obtained by resonant x-ray magnetic circular dichroism measured at the Fe L_3 edge, with dark or bright contrast corresponding to the orientation of moments in the nanomagnets, either pointing towards or away from the x-ray propagation direction, respectively. *In situ* heating of the sample was carried out using resistive filament placed directly under the sample. After setting the initial state with a magnetic field [see Figs. 1 and 2(a)], thermal relaxation of the nanomagnet arrays was performed by gradually increasing the temperature of the sample from 168 to 288 °C over a period of
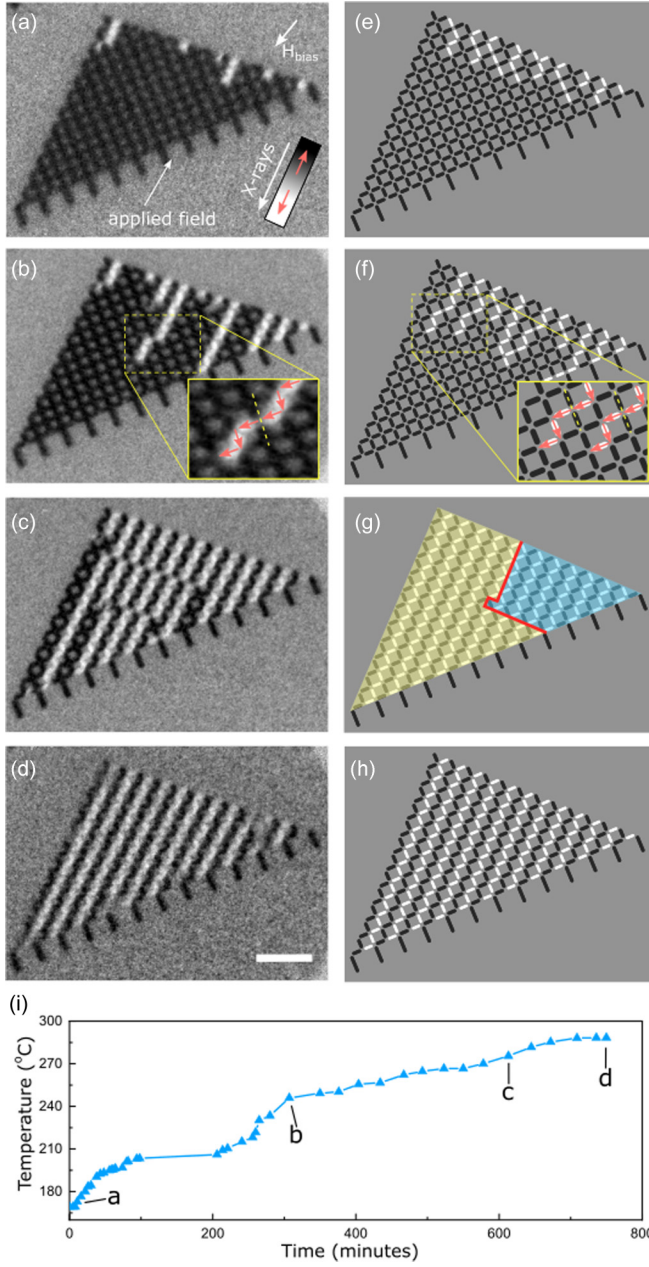
FIG. 2. Magnetization dynamics in the $v2$-$v4$ structure. X-PEEM images (a)–(d), accompanied by Monte Carlo simulations (e)–(h), displaying the monopole injection and the subsequent monopole currents. (a), (e) The magnetic moments initially point towards the direction of the applied magnetic field and, when the field is removed, injection of monopoles is restricted to the $v2$-1 edge. A 30–50-μT field is present in the X-PEEM chamber, which restricts the switching at the $v2$-1 sites to nanomagnets parallel to this field. (b), (f) Shifting of monopole currents within the structure. Shown in the inset is a close-up of shifting of a monopole current. (c), (g) The creation of domains and domain boundaries as more monopole currents shift within the structure. (d), (h) Ground state of the $v2$-$v4$ structure. (i) The thermal protocol implemented during the course of the experiment with the temperature indicated at which the X-PEEM images were taken. Scale bar is 2μm.

12.5 h for a nanomagnet thickness of ∼5.5 nm [see Fig. 2(i)]. It should be noted that the X-PEEM images in Fig. 2 were obtained by averaging a sufficient number of images (20–100) to obtain a good magnetic contrast. Such an averaging across multiple images would also mean that some nanomagnets in the averaged X-PEEM image have a gray contrast due to the possible thermal fluctuations of the magnetic moments, as observed in Fig. 2(d).

Monte Carlo simulations were carried out using the following modified Hamiltonian of general multipolar interaction in spherical coordinates incorporating higher-order magnetostatic contributions in arrays of nanomagnets:

$$H = \frac{1}{4\pi\mu_0} \sum_{\substack{A \neq B \\ l_A l_B m_A m_B}} T_{l_A l_B m_A m_B}(\vec{R}_{AB}) Q^A_{l_A m_A} Q^B_{l_B m_B}, \quad (1)$$

where $Q^A_{l_A m_A}$ and $Q^B_{l_B m_B}$ are the moments of multipoles A and B expressed in spherical harmonics [34,35] and $T_{l_A l_B m_A m_B}(\vec{R}_{AB})$ is the geometric interaction tensor depending on the interparticle distance vector $\vec{R}_{AB}$ between multipoles on sites A and B

$$T_{l_A l_B m_A m_B}(\vec{R}_{AB})$$
$$= (-1)^{l_B} I^*_{l_A+l_B\ m_A+m_B}(\vec{R}_{AB})$$
$$\times \sqrt{\frac{(l_A + l_B - m_A - m_B)!}{(l_A - m_A)!(l_B - m_B)!} \frac{(l_A + l_B + m_A + m_B)!}{(l_A + m_A)!(l_B + m_B)!}}, \quad (2)$$

where the dependency on the distance between multipoles is given by the complex conjugate of the irregular normalized spherical harmonic function:

$$I_{l m}(\vec{r}) = \sqrt{\frac{4\pi}{2l+1}} \frac{Y_{l\,m}(\theta, \varphi)}{r^{l+1}}. \quad (3)$$

Similar to the experiment, an initial state is set with the moments in nanomagnets in the arrays pointing toward the same direction [see Fig. 2(e)]. At each Monte Carlo step, the magnetization of a randomly chosen dipole (or multipole when considering higher-order contributions) is switched and the magnetic multipole moment of a nanomagnet with reversed magnetization is then recalculated on the basis of the formulae given in Ref. [36] and the new energy calculated using Eq. (1). The new configuration is accepted or rejected in the framework of the Metropolis algorithm [34]. Samples consisting of up to 1000 lattice sites of rectangular shape with open and periodic boundary conditions were used. Lattices of triangular shape that were used in experiments were calculated using open boundary conditions. For the statistical evaluation, several runs with different seed numbers were analyzed for each nanomagnet geometry.

Nanomagnets are assumed to have dimensions of 470 nm × 200 nm, with a reference thickness (t_r) of 9 nm. The magnetic moment of a nanomagnet has been approximated to be $\mu_s = \frac{lwt}{a^3}\mu$, where l is the length, w is the width, and t is the thickness of a nanomagnet, with the lattice constant $a = 0.25$ nm and $\mu \sim \mu_B$. The energy barrier is estimated to

be $\Delta E = E_2 - E_1$ with E_1 the magnetostatic energy of vn-X vertex nanomagnets at the edge of a saturated sample and E_2 the dipolar energy of the very same vn-X vertex nanomagnet with reversal of the magnetization in one of the nanomagnets resulting in the injection of a monopole. The magnetostatic energy has been calculated on the basis of the expression $E_i = \frac{\mu_0 \mu_s^2}{4\pi a^3} \sum_j \frac{\bar{S}_i \cdot \bar{S}_j}{r_{ij}^3} - \frac{3(\bar{S}_i \cdot \bar{r}_{ij})(r_{ij} \cdot \bar{S}_j)}{r_{ij}^5}$, where $\bar{S}_i = \bar{\mu}_i / \mu_s$ is the direction of magnetic moment at site i, r_{ij} the vector between the nanomagnets for pure dipoles or on the basis of Eq. (1) if octopolar contributions have been included. The probability of the injection can be then easily estimated from $p \sim e^{-\Delta E / kT}$, where k and T are the Boltzmann constant and temperature.

IV. CONTROLLED INJECTION OF MONOPOLE CURRENTS

We now demonstrate experimentally that this structure indeed results in the controlled injection of monopole currents, imaging the magnetic configurations with X-PEEM [37]. First the initial state of the nanomagnets is set with all magnetic moments pointing towards the direction of an applied magnetic field [dark contrast in Fig. 2(a)]. Here, the magnetic field, ~60 mT, is applied at 45° to long axis of the nanomagnets as indicated in the figure. Then the field is turned off, and the sample is heated to allow spontaneous moment reorientations and relaxes to a low-energy state. It can be seen that the injection of monopoles is restricted to the $v2$-1 edge, while the $v4$-1* edge remains unperturbed [Fig. 2(a) and Supplemental Material Fig. 1 [38]]. The remaining edge is energetically protected, since it is in a low-energy $v2$-2 configuration as a natural consequence of the globally applied magnetic field [Fig. 1(b)].

We observe four distinct regimes in the monopole dynamics: (i) injection of monopoles at the $v2$-1 edge [Fig. 2(a)], followed by (ii) a fast-paced current that shifts within the structure [Fig. 2(b)], then (iii) the formation of domains [Fig. 2(c)], and finally relaxation to the ground state [Fig. 2(d)]. The thermal protocol implemented during the course of the experiment is shown in Fig. 2(i), in which the temperatures corresponding to images captured for each regime are indicated. Additional details on the thermal protocol are found in the Methods section and a more detailed set of images showing different stages of the monopole current evolution are available in Supplemental Material Fig. 1. Shifting of monopole currents, within the context of this work, corresponds to a change in moment orientation in individual nanomagnets away from a low-energy configuration. An example of such a shifting in the monopole currents is shown in the inset of Fig. 2(b). Here a monopole current jumps or shifts by one lattice and continues to propagate towards the $v4$-1* configuration edge. It should be noted that a 30–50-μT magnetic field is present in the microscope chamber [33] and thus nucleation of monopoles at the $v2$-1 site is further restricted to the reversal of nanomagnets with moments closely aligned to the direction of this small bias field. In addition, we believe that optimizing the lattice spacing, shape of the nanomagnets, and lattice size will lead to a more ordered relaxation, in which the propagation of monopole currents will be restricted to
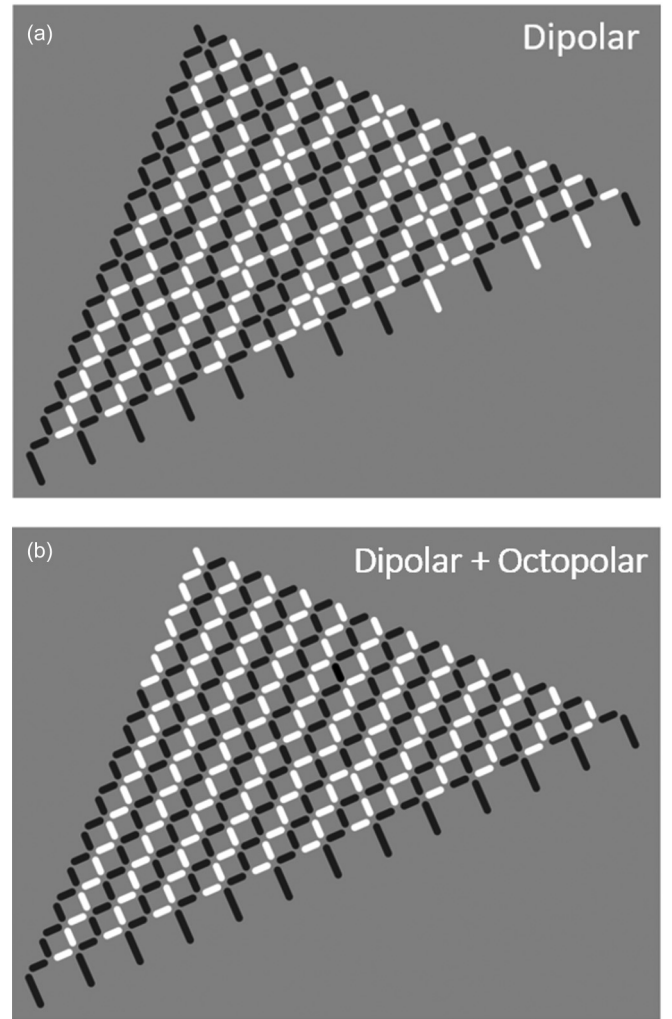

FIG. 3. Direct comparison of the effect of higher-order contributions to the magnetic Hamiltonian on the magnetic configuration at equal Monte Carlo steps. Magnetic ordering in $v2$-$v4$ structure, in which (a) only the dipolar contribution is considered and (b) the higher-order contributions, in the form of octopolar terms, are taken into account. A visual comparison between (a) and (b) demonstrates that, for a Hamiltonian with octopolar contributions, large ground-state domains are formed, which corresponds to the experimentally observed results

single lines. A movie of the dynamics is provided as part of Supplemental Material video [38].

From the Monte Carlo simulations, we find that the experimentally observed magnetization dynamics, especially the occurrence of large stable domains, is reproduced when including octopolar contributions in addition to dipolar contributions for the magnetostatic energy term in the magnetic Hamiltonian [Figs. 2(e)–2(h)]. Indeed, we have calculated analytically that the energy gain when going from an initial field-set state to that of a ground state in a $v2$-$v4$ structure is ~4 times larger when considering a Hamiltonian containing additional octopolar contributions (see Supplemental Material Fig. 2). Without the octopolar contributions, we find that, instead of the development of large domains comprising shifted currents in the $v2$-$v4$ structure, a statistical distribution of
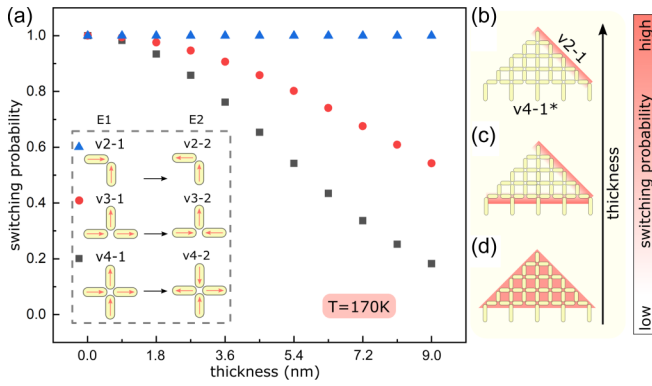
FIG. 4. Role of thickness on the location of monopole injection. (a) The probability of switching different vertex configurations, $p \sim e^{-(\Delta E)/(kT)}$, from a field-set state (vn-1) to a state with once-reversed magnet, resulting in the injection of a monopole, as a function of nanomagnet thickness at a temperature of 170 K. (b)–(d) Schematic of the regions of monopole injection in artificial square-ice structure where the red shading indicates a region of high-switching probability. It should be noted that $v4$-X corresponds to an intermediate state that is one spin flip away from $v4$-1. Shown are schematics of experimentally observed high-switching probability regions for nanomagnets with (b) large thickness, (c) medium thickness, and (d) small thickness.

shifted currents is observed (see Fig. 3). Finally, our simulations indicate that the presence of a small field in the X-PEEM chamber is not sufficient to explain the large domain formation observed in the experiment.

V. SWITCHING PROBABILITIES

We address here the influence of the nanomagnet thickness on the injection location of monopoles in artificial spin-ice structures. The initial state in arrays of different thickness was set with a globally applied magnetic field as described earlier. Here the moment configurations in the nanomagnets were not allowed to fully relax to the ground state but were rather frozen into an intermediate energy configuration, which allowed us to qualitatively reveal the role of thickness in influencing the location of monopole injection. We observed three distinct thickness regimes, which result in monopole injection at different locations in an artificial spin-ice structure. These regimes are as follows: (i) at a thickness of $\sim$3 nm [Supplemental Material Fig. 3, images (a)–(d)], the monopole injection occurred at any location in the array, (ii) at an increased thickness of $\sim$4 nm (Supplemental Material Fig. 3, images (e)–(h), monopole injection is restricted to the edges containing $v2$-1, $v3$-1, and $v4$-1 vertices, and (iii) at a higher thickness of $\sim$5.5 nm, monopole injection was highly restricted to $v2$-1 vertices (Fig. 2).

This strong correlation between the nanomagnet thickness, vertex configurations, and location of monopole nucleation can be understood by determining the probability of nucleation of a monopole at different vertex configurations (see Methods). It can be seen from Fig. 4(a) that a $v2$-1 configuration (solid blue triangles) has a higher switching probability compared to a $v3$-1 configuration (solid red circles) or a $v4$-1 configuration (solid black squares). This difference in the switching probability is essential to induce directional injection of monopole currents at $v2$-1 sites in an asymmetric nanomagnet array such as the $v2$-$v4$ structure. Considering the Boltzmann probability of a transition between different vertex configurations ($\sim e^{-\Delta E/kT}$) given in Fig. 4(a), we indicate the regions of high probability for switching, and therefore monopole nucleation, in a $v2$-$v4$ structure for different thicknesses in Figs. 4(b)–4(d). Here, the injection events are restricted to the $v2$-1 sites for high thickness [Fig. 4(b)], $v2$-1 and $v3$-1 sites (i.e., $v4$-1* edge) for medium thickness [Fig. 4(c)] and occur everywhere in the structure for low thickness [Fig. 4(d)]. The calculated probabilities for monopole nucleation and supporting the schematics in Fig. 4(b) are therefore in good agreement with the experimentally observed results.

VI. CONCLUSIONS

We have demonstrated that monopoles can be injected with a high degree of control in an artificial square ice. In particular, the injection of monopoles is strongly dependent on the vertex configurations at an edge of an artificial spin-ice structure. Furthermore, the large domains observed in the experiments can be attributed to higher-order octopolar contributions in the magnetic Hamiltonian. The strong correlation between the location of an injection site, film thickness, and vertex configuration at an edge is captured in a plot of the switching probabilities. The control of the location of injection of monopoles and the subsequent generation of monopole currents is an important step towards the realization of devices with monopole currents for use in applications such as computation [32,33].

[1] C. Nisoli, R. Moessner, and P. Schiffer, Rev. Mod. Phys. **85**, 1473 (2013).

[2] L. J. Heyderman and R. L. Stamps, J. Phys. Condens. Matter **25**, 363201 (2013).

[3] S. H. Skjærvø, C. H. Marrows, R. L. Stamps, and L. J. Heyderman, Nat. Rev. Phys. **2**, 13 (2020).

[4] R. F. Wang, C. Nisoli, R. S. Freitas, J. Li, W. McConville, B. J. Cooley, M. S. Lund, N. Samarth, C. Leighton,

V. H. Crespi, and P. Schiffer, Nature (London) **439**, 303 (2006).

[5] A. Farhan *et al.*, Phys. Rev. Lett. **111**, 057204 (2013).

[6] L. A. Mól, R. L. Silva, R. C. Silva, A. R. Pereira, W. A. Moura-Melo, and B. V. Costa, J. Appl. Phys. **106**, 063913(R) (2009).

[7] G. Möller and R. Moessner, Phys. Rev. B **80**, 140409(R) (2009).

[8] E. Mengotti, L. J. Heyderman, A. Fraile Rodriguez, A. Bisig, L. Le Guyader, F. Nolting, and H. B. Braun, Phys. Rev. B **78**, 144402 (2008).

[9] C. Castelnovo, R. Moessner, and S. L. Sondhi, Nature (London) **451**, 42 (2008).

[10] E. Mengotti, L. J. Heyderman, A. F. Rodriguez, F. Nolting, R. V. Hugli, and H.-B. Braun, Nat. Phys. **7**, 68 (2011).

[11] Y. Perrin, B. Canals, and N. Rougemaille, Nature (London) **540**, 410 (2016).

[12] A. Farhan, M. Saccone, C. F. Petersen, S. Dhuey, R. V. Chopdekar, Y. L. Huang, N. Kent, Z. Chen, M. J. Alava, T. Lippert, A. Scholl, and S. V. Dijken, Sci. Adv. **5**, eaav6380 (2019).

[13] E. Y. Vedmedenko, Phys. Rev. Lett. **116**, 077202 (2016).

[14] S. Ladak, D. E. Read, W. R. Branford, and L. F. Cohen, New J. Phys. **13**, 063032 (2011).

[15] S. T. Bramwell, S. R. Giblin, S. Calder, R. Aldus, D. Prabhakaran, and T. Fennell, Nature (London) **461**, 956 (2009).

[16] A. Imre, G. Csaba, L. Ji, A. Orlov, G. H. Bernstein, and W. Porod, Science **311**, 205 (2006).

[17] R. P. Cowburn and M. E. Welland, Science **287**, 1466 (2000).

[18] J. Grollier, D. Querlioz, and M. D. Stiles, Proc. IEEE **104**, 2024 (2016).

[19] B. Lambson, D. Carlton, and J. Bokor, Phys. Rev. Lett. **107**, 010604 (2011).

[20] J. Hong, B. Lambson, S. Dhuey, and J. Bokor, Sci. Adv. **2**, e1501492 (2016).

[21] R. V. Hügli, G. Duff, B. Conchuir, E. Mengotti, A. F. Rodríguez, F. Nolting, L. J. Heyderman, and H. B. Braun, Philos. Trans. R. Soc., A **370**, 5767 (2012).

[22] S. Gliga, A. Kákay, R. Hertel, and O. G. Heinonen, Phys. Rev. Lett. **110**, 117205 (2013).

[23] S. Lendinez and M. B. Jungfleisch, J. Phys.: Condens. Matter **32**, 013001 (2019).

[24] E. Iacocca, S. Gliga, and O. G. Heinonen, Phys. Rev. Appl. **13**, 044047 (2020).

[25] D. Thonig and J. Henk, J. Magn. Magn. Mater. **386**, 117 (2015).

[26] A. León, Physica B **500**, 59 (2016).

[27] J. Drisko, T. Marsh, and J. Cumings, Nat. Commun. **8**, 14009 (2017).

[28] S. Krishnia, I. Purnama, and W. S. Lew, J. Magn. Magn. Mater. **420**, 158 (2016).

[29] Z. Budrikis, J. P. Morgan, J. Akerman, A. Stein, P. Politi, S. Langridge, C. H. Marrows, and R. L. Stamps, Phys. Rev. Lett. **109**, 037203 (2012).

[30] S. A. Morley, Ph.D. Thesis, The Dynamics of Artificial Spin Ice in Real and Reciprocal Space, University of Leeds, 2015.

[31] S. A. Morley *et al.*, Sci. Rep. **9**, 15989 (2019).

[32] H. Arava, M. D. Peter, V. Jaianth, C. Jizhai, S. B. Nicholas, K. Armin, and J. H. Laura, Nanotechnology **29**, 265205 (2018).

[33] H. Arava, N. Leo, D. Schildknecht, J. Cui, J. Vijayakumar, P. M. Derlet, A. Kleibert, and L. J. Heyderman, Phys. Rev. Appl. **11**, 054086 (2019).

[34] E. Y. Vedmedenko, N. Mikuszeit, H. P. Oepen, and R. Wiesendanger, Phys. Rev. Lett. **95**, 207202 (2005).

[35] E. Y. Vedmedenko and N. Mikuszeit, ChemPhysChem **9**, 1222 (2008).

[36] M. Schult, N. Mikuszeit, E. Y. Vedmedenko, and R. Wiesendanger, J. Phys. A Math. Theor. **40**, 14791 (2007).

[37] L. Le Guyader, A. Kleibert, A. Fraile Rodríguez, S. El Moussaoui, A. Balan, M. Buzzi, J. Raabe, and F. Nolting, J. Electron Spectrosc. Relat. Phenom. **185**, 371 (2012).

[38] See Supplemental Material at http://link.aps.org/supplemental/10.1103/PhysRevB.102.144413 for X-PEEM images of the monopole dynamics.

[39] https://doi.org/10.5281/zenodo.4014612.